Print ISSN: 0375-9237
Online ISSN: 2357-0350

EGYPTIAN JOURNAL OF BOTANY (EJBO)

Aspergillus detection based on deep learning model using YOLOv8 with a small custom dataset

Hossam M. Hassan, Asmaa Amir, Mohamed N. Abd El-Ghany, Said A. Saleh, Khaled F. El-Yasergy, Salama A. Ouf

PUBLISHED BY
THE EGYPTIAN
BOTANICAL SOCIETY

Aspergillus detection based on deep learning model using YOLOv8 with a small custom dataset

Hossam M. Hassan[1], Asmaa Amir[2], Mohamed N. Abd El-Ghany[3], Said A. Saleh[4], Khaled F. El-Yasergy[3], Salama A. Ouf[3]

[1]Department of Mathematics, Faculty of Science, Cairo University, Giza 12613, Egypt
[2]Department of Biotechnology, Faculty of Science, Cairo University, Giza 12613, Egypt
[3]Botany and Microbiology department, Faculty of Science, Cairo University, Giza 12613, Egypt
[4]Department of Chemistry, Faculty of Science, Cairo University, Giza 12613, Egypt

Over the past years, there has been a growing interest in studying the effects of fungal respiratory diseases by the predominant species identified in respiratory cultures from this genus *Aspergillus.* Machine learning autonomously identifies the five distinct species of *Aspergillus*. We selected a diverse array to show a wide array of color combinations, dimensions, and configurations, which enhance the incorporation of diversity and intricacy in our research. The split was conducted in a random manner, allocating 70% of the data to the training set, 20% to the validation set, and 10% to the test set. The heterogeneity among various forms of *Aspergillus* was assessed based on the photos. The photographs were taken against two distinct backgrounds: one in copper and the other in grey color. Multiple elevations and shooting angles were taken into consideration. The crowdedness of the *Aspergillus* also varied randomly per image. We utilized a smartphone camera boasting a resolution of 32 megapixels. A grand total of 337 photographs were captured, including five *Aspergillus* species that were appropriately identified. CSPDarknet53 acts as the fundamental structure for YOLOv8, which is constructed on top of DenseNet. The YOLOv8 model attained a mean average precision (mAP) of 90%. YOLOv8 has a significant advantage in terms of its speed in detecting objects, making it suitable for real-time identification situations that demand both high accuracy and few false positives. The results demonstrated that YOLOv8 exhibited outstanding precision and detection performance. This technique is highly effective and efficient in detecting many species of *Aspergillus*.

ARTICLE HISTORY
Submitted: December 05, 2024
Accepted: February 12, 2025

CORRESPONDENCE TO
Mohamed N. Abd El-Ghany,
Botany and Microbiology department,
Faculty of Science, Cairo University,
Giza 12613, Egypt
Email: mabdelghany@sci.cu.edu.eg
DOI: 10.21608/ejbo.2025.342052.3109

EDITED BY: N. Khalil

Keywords: *Aspergillus* species, machine learning, YOLOv8, DenseNet, CSPDarknet53, validation

INTRODUCTION

Fungi represents the third most varied category of eukaryotic organisms on Earth, with around 140,000 identified species, while estimates range from 700,000 to 12 million. Fungi inhabits terrestrial, freshwater, and marine habitats. In these environments, these organisms contribute towards significant diseases for humans, animals, and plants, as well as acting as crucial agents for carbon and nutrient recycling (Oliveira and Azevedo, 2022).

Aspergillus comprises more than 340 officially acknowledged species, categorized according to their physical characteristics, biological functions, and evolutionary qualities. These classifications have considerable significance in diverse areas like agricultural production, biotechnology, environmental science, and human health. *Aspergillus fumigatus* is both a potentially deadly human infection and a significant allergen. It has attracted attention due to its connection with allergic reactions and invasive disorders (Qi et al., 2024). *Aspergillus* species commonly cause invasive fungal infections in patients with weak immune systems. They are also linked to allergic bronchopulmonary illnesses, mycotic keratitis, otomycosis, and nasal sinusitis. There are a minimum of 30 *Aspergillus* species that have been linked to illnesses in humans (Diba et al., 2007).

Aspergillus spp. spores are primarily disseminated through the air. Consequently, human airways are the primary organ at risk for *Aspergillus* infection, particularly in people with preexisting sinus or pulmonary conditions. Individuals with compromised natural immunity (e.g., inability to expel secretions) or cellular immunity (e.g., neutropenia, diminished T cell function, and immunosuppressive medications) are more vulnerable and may experience fast advancing diseases that might lead to grave consequences (Dobiáš et al., 2023). Fungi are essential constituents of soil microbiota and play a key role in soil ecosystem functioning, especially in forest and agricultural soils. *Aspergillus* has a role in the cycling of major nutrients, especially its potential role in the decomposition of complex organic molecules (Rakiya et al., 2024). Vegetables are vital preventative foods that promote health maintenance and illness prevention; yet, certain fungus, including *Penicillium* spp., *Aspergillus* spp., and *Fusarium* spp., can proliferate on vegetables and contaminate them (Al-Ameri, 2024). The *Aspergillus* genus is highly significant among filamentous fungal genera. *Aspergillus* species are utilized in the fermentation industry, but they can also cause secondary roots in plants and food due to the potential buildup of mycotoxins. While *Aspergillus* species are not typically regarded as a primary cause of plant disease,

they do contribute to multiple problems in different plants and plant products (Perrone et al., 2007).

Enhancing the identification of physical features of opportunistic fungi in stained samples through microscopic analysis, optimizing the growth rate and conidia production of *Aspergillus* spp. in laboratory cultures, and identifying unusual variations of common aspergilli can enhance the laboratory's ability to provide quick diagnoses (McClenny, 2005). According to a 2003 survey conducted by the American Society for Microbiology (ASM) on the identification of microbial pathogens, 89% of laboratories that perform morphology-based mycological examinations use serologic tests, while fewer than 5% use molecular tests. The survey specifically focused on the isolation and phenotypic identification of common clinical *Aspergillus* spp. Isolates are comparatively faster to trigger intricate host diseases. The applications in microbiology are rapidly developing, and the machine learning methods commonly employed in basic and clinical research encompass a wide range of techniques, including classification, regression, clustering, and dimensionality reduction (Asnicar et al., 2024). Applying machine learning algorithms to spam filtering focuses on textual and image-based approaches instead of considering spam filtering as a standard classification problem (Guzella and Caminhas, 2009). Machine learning approaches play an essential role in analyzing spectrum data for spectroscopy and imaging systems. Deep learning is currently a widely discussed subject in the field of artificial intelligence, and convolutional neural networks (CNNs) have emerged as one of the most often used and favored models within the realm of deep learning. Traditionally, deep learning techniques have been employed for the analysis of two-dimensional images (Qiu et al., 2018). The primary method utilized for identifying and displaying signs of plant diseases from color photographs was computer vision. The features retrieved from these images were then used as inputs for other classifiers, including the Support Vector Machine Classifier (Camargo and Smith, 2009). Machine learning involves the direct examination of digital photographs or scans of groupings of things. By incorporating pixel brightness and color values as variables in morphometric analysis, the traditional approach of geometric morphometrics (GM) becomes more effective and allows for an analysis of all points that make up the object that is being investigated. Matrices are constructed and group partitioning is performed using logistic regression. Geometric morphometrics and form analysis algorithms are currently advised for conducting several analyses on a single collection of objects and generating the corresponding findings, notwithstanding some oversimplifications. Precise information regarding the color distribution, size, and textural measurements of the fungal colony can be extracted from a digital photograph (MacLeod, 2017). From a clinical perspective, it may be required to identify unknown *Aspergillus* isolates to the species level because different species exhibit varying susceptibilities to diverse antifungal medications (Balajee et al., 2007).

MATERIALS AND METHODS

Fungal Isolation, Growth Media, and Culture Conditions

The current investigation involved the isolation of fungal species from an agricultural soil in Giza, Egypt, utilizing the soil dilution plate method as described by Johnson et al. (1960). Inoculum from soil samples was applied onto Czapek-Dox agar (CZA) medium, which consisted of the following components per liter: 20 g of sucrose, 2 g of $NaNO_3$, 1 g of K_2HPO_4, 0.5 g of KCl, 0.5 g of $MgSO_4.7H_2O$, 0.01 g of $FeSO_4.7H_2O$, and 15 g of agar. After sterilization and cooling, the previously filtered streptomycin solution (30 mg/mL) was added to the medium mentioned above. The fungal colonies were purified using the streak plate method. Subsequently, the identification of the specimens was conducted by assessing their morphological and microscopic attributes, such as color, texture of mycelia, and spore production pattern. This assessment was carried out following the methods described by Gilman (1957), Raper (1965), Moubasher (1993), and Watanabe (2002). The fungal species were cultivated on slants with CZA medium at a temperature of 28 degrees Celsius for a duration of 4 days. The spores from each strain were collected and preserved at a temperature of 4°C in a sterile solution of spore suspension buffer, which consisted of 0.9% (w/v) NaCl and 1% (v/v) Tween 80(Khalil et al., 2019). We selected five distinct species of *Aspergillus* fungus as the subjects for our investigation. These selections exhibit varying sizes and shapes to introduce diversity and intricacy into our research. The study used a dataset of images of the *Aspergillus* fungus. Since this dataset is not publicly available like other datasets used in machine learning and computer vision research (such as ImageNet, PASCAL VOC, and COCO), it was manually collected, annotated, and then divided randomly into three sub-

datasets: train, validation, and test (predictions). The ratio of images in each sub-dataset is 80%, 10%, and 10%, respectively.

Molecular Identification of Fungal Isolates

The detection of *Aspergillus terreus, Aspergillus fumigatus*, *Aspergillus flavus*, *Aspergillus welwitschiae*, and *Aspergillus austwickii* was additionally verified by analyzing the nuclear ribosomal DNA internal transcribed spacer (ITS) sequence. The genomic DNA was acquired via the methodology outlined in the GeneJet Plant genomic DNA purification Kit (Thermo) no. K0791, which may be found at http://www.thermoscientificbio.com. The genetic sequence includes the 18S ribosomal RNA gene, the internal transcribed spacer 1, the 5.8S ribosomal RNA gene, the internal transcribed spacer 2, and the 28S ribosomal RNA gene. The target gene is the 18S ribosomal RNA gene, which includes the internal transcribed spacer 1, the 5.8S ribosomal RNA gene, the internal transcribed spacer 2, and the 28S ribosomal RNA gene. The length of the amplified gene is 564 base pairs (bp), with sequencer reading length of 324. The primers used are ITS1 with sequence (CTT GGT CAT TTA GAG GAA GTA A) and ITS4 with sequence (TCC TCC GCT TAT TGA TATGC).

The obtained sequence was inputted into the BLAST algorithm of the National Center of Biological Information (NCBI) database to retrieve closely related phylogenetic sequences. A phylogenetic tree was generated using the BLAST algorithm. The acquired sequence was then uploaded to the GenBank database of the National Center for Biotechnological Information (NCBI). Each isolate was assigned a strain identifier and an accession number. A phylogenetic tree was generated via MEGA 11 software. The acquired sequence was subsequently uploaded to the GenBank database of the National Centre for Biotechnology Information (NCBI). Each isolate was assigned a strain identifier and an accession number.

Image Collection

The images for our dataset were gathered through manual collection. The photos were examined to assess the variety among several species of fungi. The study focuses on five specific types of *Aspergillus* fungus: *Aspergillus terreus*, *Aspergillus fumigatus*, *Aspergillus flavus*, *Aspergillus welwitschiae*, and *Aspergillus austwickii*. The images were taken against two distinct backgrounds: one of copper and the other of grey color. Alternative elevations and shooting perspectives were considered. The density of *Aspergillus* also exhibited random variation in each photograph. The imaging tool employed is a smartphone camera boasting a resolution of 32 megapixels. A total of 337 pictures were acquired, which included 5 labeled objects. The dataset comprised photos with diverse backgrounds, heights, angles, crowdedness, layouts, and combinations, as depicted in Figure 1.

Object Annotation

Object detection, often called object recognition, is the exact identification and localization of an object within an image. A tool for object annotation was utilized to assign labels to the collected photographs. The LabelImg tool, created by Tzutalin and accessible at https://github.com/tzutalin/labelImg, was selected from a collection of often utilized utilities including LabelImg, Imglab, LabelMe, Labelbox, and RectLabel. The image annotations were saved in two file formats: .txt, which is the input format for YOLO, and .xml, which is compatible with the prior to being input into the models; all photos in our dataset underwent preprocessing. The primary preprocessing step involved adjusting the input image resolution to ensure compatibility with our models, hence preventing memory issues, slow processing speed, and reduced accuracy. PASCAL VOC dataset can be easily converted into TF records.

Data Standardization

We applied the Darknet deep learning framework to create the YOLOv8 model. After being prepared, the photos and annotations data were fed into the model. Subsequently, the dataset was divided into train, validation, and test sets using random selection, with proportions of 70%, 20%, and 10%, respectively.

Preprocessing and Network Models

Every object detector has a central support, cervical region, and sensing component. Initially, the input image is passed via the backbone, which utilizes a convolutional neural network to condense the characteristics. Contrary to picture classification, object detection backbones do not serve as the last component of the network. Predictions cannot be solely based on them; localization must be combined with classification. Localization involves the process of determining the precise location of an item in an image by drawing numerous bounding boxes. This requires the feature layers of the convolutional backbone to be combined and coordinated with one other.

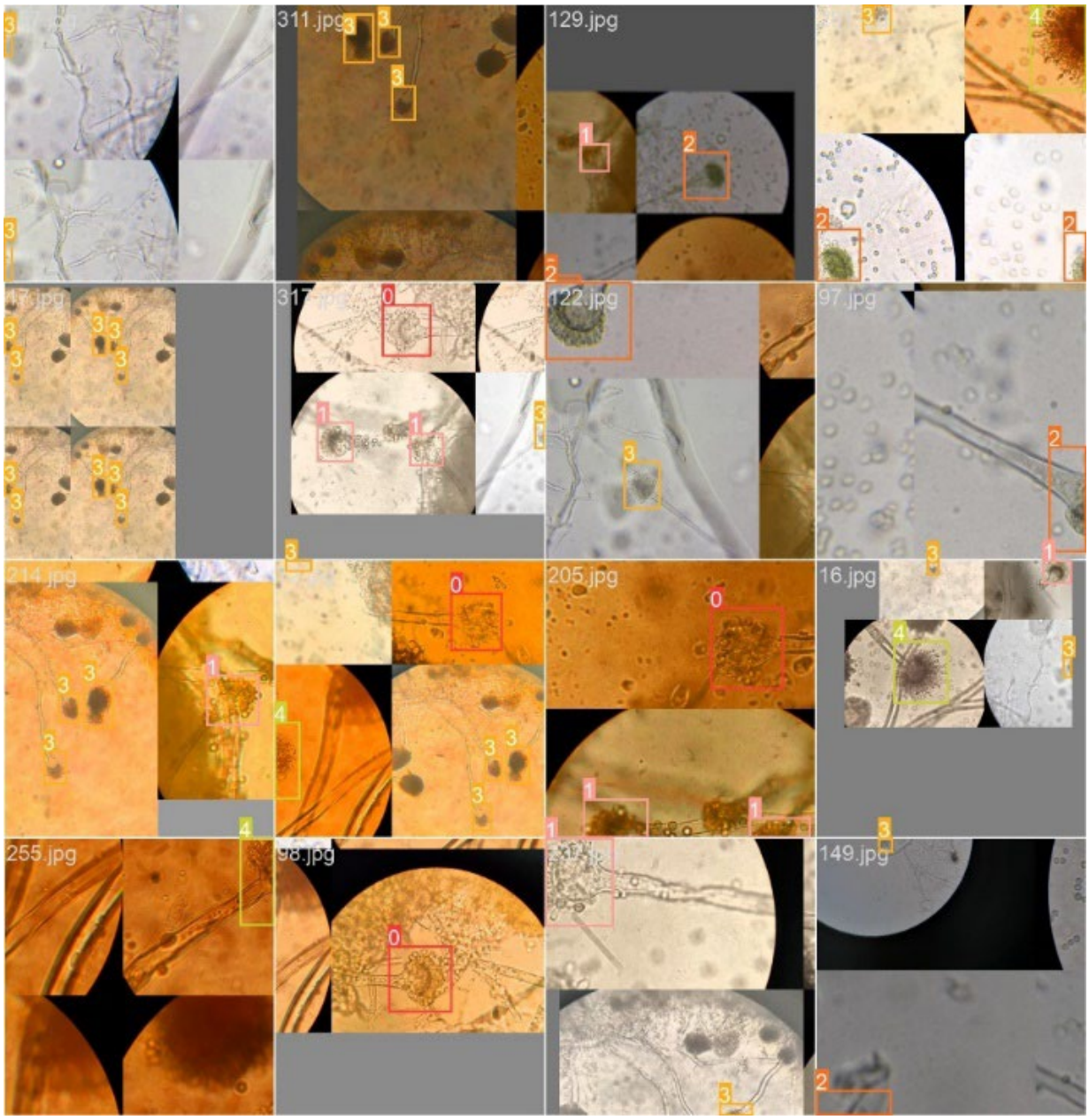

Figure 1. The different samples used in the dataset.

The fusion of primary structural layers occurs in the cervical region, followed by the identification process in the cranial region. It is beneficial to categorize object detectors into two groups: one-stage detectors and two-stage detectors, as illustrated in Bochkovskiy et al. (2020). Two-stage detectors separate the process of object localization and classification for each bounding box, whereas one-stage detectors do object localization and classification concurrently.

YOLOv8

The YOLO (You Only Look Once) series of models has gained renown in the field of computer vision. The success of YOLO can be attributed to its exceptional accuracy, despite its little model size. YOLO models may be trained using only one GPU, which makes it easily accessible to a diverse group of developers. Machine learning practitioners have the option to utilize it on inexpensive edge hardware or in the cloud. The computer vision community has actively supported and developed YOLO since its initial

release in 2015 by Joseph Redmond. During the initial stages (versions 1-4), YOLO was upheld in C code within a specialized deep learning framework known as Darknet, developed by Redmond. YOLO (versions 1-4) has proven its efficiency beating other popular models like Faster R-CNN at accuracy and speed (Ouf, 2023). Over the past two years, other models have emerged from the YOLOv5 PyTorch repository, such as Scaled-YOLOv4, YOLOR, and YOLOv7. Several PyTorch-based implementations of models, including YOLOX and YOLOv6, were developed in different parts of the world. Throughout their development, each YOLO model has introduced state-of-the-art (SOTA) techniques that consistently enhance the accuracy and efficiency of the model. Ultralytics conducted research on the latest state-of-the-art (SOTA) iteration of YOLO, known as YOLOv8, for a period of six months. YOLOv8 was released on January 10, 2023. The YOLOv8 model has high accuracy on the COCO dataset. As an illustration, the YOLOv8m model, namely the medium-sized model, attains a mean average precision (mAP) of 50.2% when evaluated on the COCO dataset. When compared to Roboflow 100, a dataset designed to assess model performance in several task-specific domains, YOLOv8 outperformed YOLOv5 by a significant margin. Further details regarding YOLOv8 architecture is presented in Figure 2. Moreover, the developer-friendly functionalities of YOLOv8 are substantial. Unlike previous models that distribute tasks over multiple Python files for execution, YOLOv8 simplifies model training by providing a Command Line Interface (CLI) that enhances intuitiveness. This is an additional feature of a Python package that offers a smoother development experience compared to previous versions.

The Assessment Method

Loss Function

YOLOv8 utilizes advanced loss functions to optimize the model, which include the following:

- **CIoU loss** during training: the accuracy of localization can be improved by using bounding box regression, which is expressed as box_loss.
- **DFL loss** (Distribution Focal Loss): as correctly pointed out, the issue is specifically referred to as dfl_loss. It enhances the model's ability to more accurately predict item classifications.
- **VFL loss** (Varifocal Loss): the value is not displayed independently but rather included within the cls_loss (class loss) in the training logs. The purpose of VFL is to mitigate disparities and ambiguities in classification jobs.

Every loss component is crucial in refining the accuracy of the model, with each one specifically targeting a particular aspect of the detection task, such as localization and classification. The training logs indicate the performance of the model in several areas by displaying box loss, cls loss, and dfl loss. The objective throughout training is to minimize these losses to enhance the performance of the model (Wu et al., 2020). The loss function integrates the losses of classification and bounding box regression in the following manner:

$$L = L_{cls} + L_{box} \quad (1)$$

$$L(\{p_i\},\{t_i\}) = \frac{1}{N_{cls}}\sum_i L_{cls}(p_i, p_i^*) + \frac{\lambda}{N_{box}}\sum_i p_i^* \cdot L_1^{smooth}(t_i - t_i^*) \quad (2)$$

In this context, "i" represents the index of an anchor within a batch. "p_i" represents the anticipated probability of anchor "i" being an object. "p_i^*" represents the ground truth label, which is a binary value indicating whether anchor "i" is an object. When the anchor is a positive sample, "p_i^*" is equal to 1. When it is a negative sample, "p_i^*" is equal to 0. The regression loss term is activated only when the anchor is positive. "t_i" represents the predicted four parameterized coordinates of the positive sample anchor, while "t_i^*" represents the ground truth coordinates of the positive sample anchor. The balancing parameter "λ" is used to weigh the classification loss "L_{cls}" and the bounding box regression loss "L_{box}" so that both terms have roughly equal weight. The default value of "λ" is set to be approximately 10. "N_{cls}" and "N_{box}" are normalization terms used to normalize the classification loss item "L_{cls}" and the regression loss item "L_{box}," respectively. The log loss function, denoted as L_{cls}, is used to measure the error in binary classification. It may also be applied to multiclass classification by converting it into a binary classification problem, where we forecast whether a sample belongs to the target class or not. The L_1 smooth loss refers to the smooth L_1 loss. The classification loss function L_{cls} is a binary classifier that determines if an object is present or not. The formula for this classifier is as follows:

$$L_{cls}(p_i, p_i^*) = -p_i^* \log p_i - (1 - p_i^*) \log(1 - p_i) \quad (3)$$

The bounding box regression loss function L_{box} is used to calculate the difference between the two transformations, and the formula is as follows:

$$L_{box}(t_i, t_i^*) = R(t_i - t_i^*) \quad (4)$$

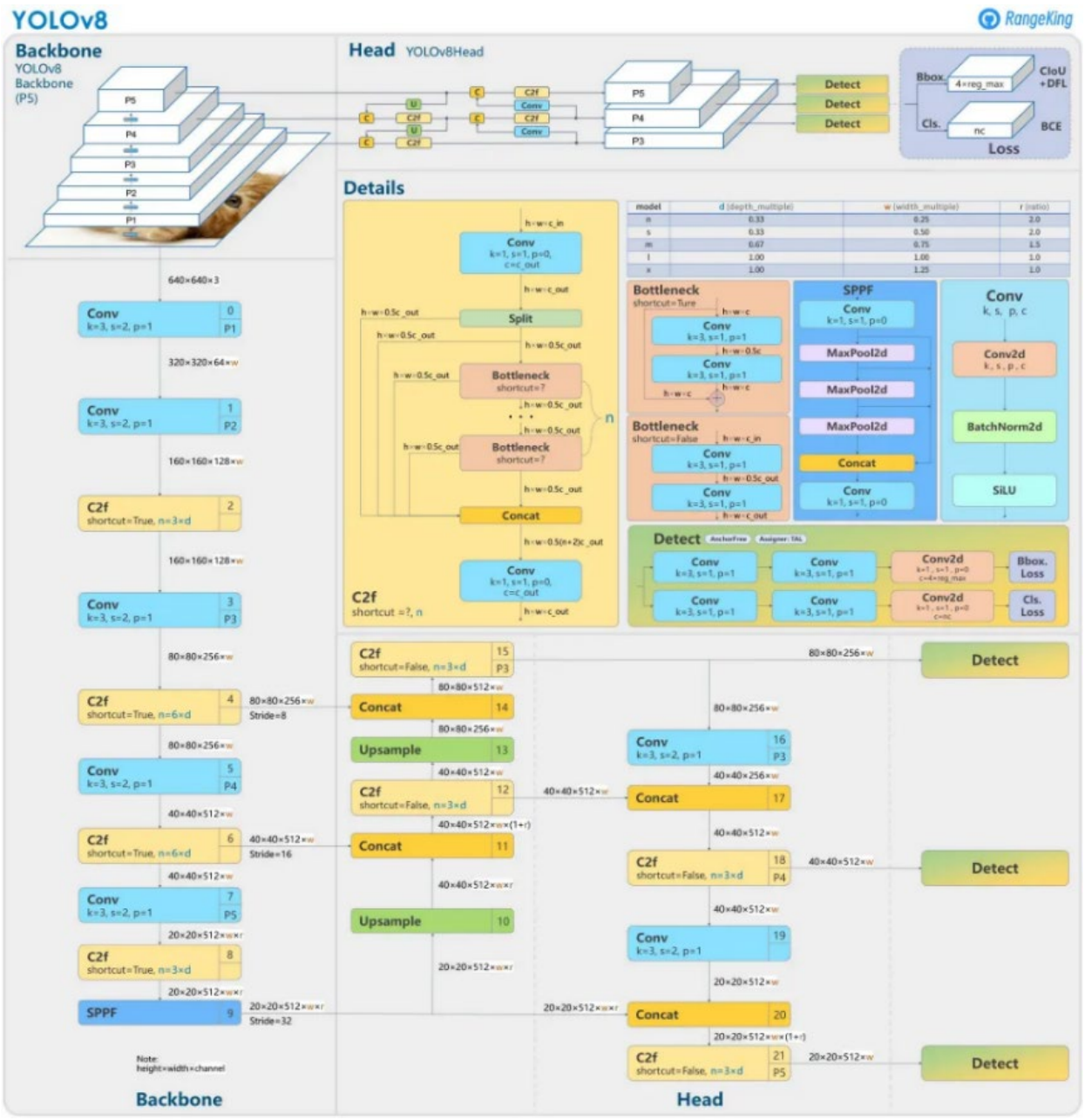

Figure 2: YOLOv8 architecture, visualization made by GitHub user RangeKing. Source: https://blog.roboflow.com/whats-new-in-yolov8

where R function is defined as

$$Smooth_{L_1}(\chi) = \begin{cases} 0.5\chi^* & ,|\chi| < 1 \\ |\chi| - 0.5 & ,otherwise \end{cases} \quad (5)$$

Precision, Recall, and mAP

The mAP is a widely used statistic for evaluating the performance of an object detection model. The topic encompasses two fundamental concepts: precision and recall. Precision, also referred to as the positive predicted value, is a measure for an item that quantifies the ratio of accurately predicted positive observations to the total number of expected positive observations. In other words, high precision indicates a low rate of false-positive predictions:

$$precision = \frac{TP}{TP+FP} \quad (6)$$

The precision and recall performance of the model can be changed by modifying the SoftMax threshold in the final layer. Raising the threshold would result in a reduction of false positives (FP), hence increasing precision and decreasing recall. Similarly, to enhance memory, it is necessary to lower the frequency of

false negatives (FN), which would consequently lead to a reduction in precision. In object detection jobs, it is typically necessary for the precision to be high, meaning that the number of anticipated positives that are true positives (TP) should be maximized. Precision and recall are commonly employed metrics in conjunction with other measures, such as accuracy, which represents the proportion of properly predicted observations to the total number of observations:

$$Accuracy = \frac{TP+TN}{TP+FP+FN+TN} \quad (8)$$

The F1 score is a metric that combines precision and recall (Huang et al., 2015). It is a more informative measure than accuracy; however, it is not as straightforward to calculate. Accuracy is a valuable indicator, particularly when dealing with datasets that are symmetrical, meaning that the costs of false positives and false negatives are equivalent. The F1 score considers both false positives and false negatives. If the costs associated with false positives and false negatives exhibit significant disparity, it is advisable to include both precision and recall metrics (Chinchor, 1992):

$$F1 - score = \frac{2 \times (recall \times precision)}{Recall + precision} \quad (9)$$

Intersection over Union (IoU) is a metric used to calculate the average precision (AP) for object detection. The Intersection over Union (IoU) is calculated by dividing the area of intersection between the predicted bounding box and the ground truth bounding box by the area of their union, as shown in the following equation:

$$IoU = \frac{Area\ Of\ Overlap}{Area\ Of\ Union} \quad (10)$$

The Intersection Over Union (IoU) metric is employed to ascertain if a predicted bounding box (BB) is classified as true positive (TP), false positive (FP), or false negative (FN). The TN (true negative) is not assessed as it is presumed that each image contains an object. Historically, the IoU (Intersection over Union) value has been conventionally established at 0.5. During the execution of the object detection model on an image, a bounding box is considered a true positive (TP) if the Intersection over Union (IoU) is more than 0.5. It is considered a false positive (FP) if either the IoU is less than 0.5 or if the bounding box is duplicated. Finally, it is considered a false negative (FN) if the item is not detected at all. If the object detection model fails to detect the target, either due to no detection or if the predicted bounding box (BB) has an Intersection over Union (IoU) greater than 0.5 but is classified incorrectly, then the predicted BB would be considered a false negative (FN). The precision and recall metrics were computed for a specific class over the test dataset. Each bounding box (BB) would possess a confidence level, often determined by its SoftMax layer, and would be utilized to prioritize the output.

Interpolated Precision

Before plotting the PR curve, it is necessary to determine the interpolated precision. The interpolated precision, P_{interp}, is determined for each recall level, r, by selecting the highest precision value obtained for that r. The formula is provided in the following manner:

$$P_{interp}(\tilde{r}) = \underset{r > \tilde{r}}{max}\, p(r) \quad (11)$$

where $p(\tilde{r})$ is the measured precision at recall $\tilde{r}$.

Their objective in interpolating the PR curve was to mitigate the influence of minor fluctuations in the ranking of detections, hence enabling the plotting of the PR curve. The precision, recall, and interpolated precision for each example are calculated using the formulas stated above. The AP is determined by computing the integral of the precision-recall curve. The recalls are evenly divided into 11 segments, ranging from 0 to 1 with increments of 0.1. We get the following:

$$\frac{1}{11} \sum_{r \in \{0,0.1,0.2,..,0.9,1\}} P_{interp}(r) \quad (12)$$

Recall, also referred to as the true-positive rate or sensitivity, is the proportion of properly predicted positive observations to the total number of observations in each class:

$$recall = \frac{TP}{TP+FN} \quad (7)$$

COCO Metrics

The COCO dataset is commonly employed for training and validating object detection models. The dataset encompasses a diverse array of 80 object categories, which aids in the model's ability to generalize. Transfer learning involves utilizing pretrained models trained on the COCO dataset to perform object detection tasks on new training data. COCO introduced six novel techniques for computing average recall (AR) and mean average precision (mAP) at various Intersection over Union (IoU) thresholds and object dimensions. The metrics include mean average precision (mAP) at an Intersection over Union

(IoU) threshold of 0.5, where the IoU of bounding boxes needs to be above 0.50. Another metric is mAP at an IoU threshold of 0.75, where the IoU of bounding boxes needs to be above 0.75. Additionally, there is mAP at various IoU thresholds ranging from 0.50 to 0.95 with an increment of 0.05. Furthermore, there is mAP specifically for small objects with an area below 32^2 pixels, mAP for medium objects with an area between 32^2 and 96^2 pixels, and mAP for large objects with an area above 96^2 pixels. The primary metric, mean average precision (mAP), is determined by computing the average precision (AP) from an initial Intersection over Union (IoU) of 0.5 to a final IoU of 0.95, with increments of 0.05. Subsequently, the results are computed by taking the average.

Additional metrics include the assessment of augmented reality (AR) performance at various object sizes and the detection of multiple instances. The metrics include the aspect ratio (AR) for small items with an area less than 32^2 px, AR for medium objects with an area between 32^2 and 96^2 px, AR for large objects with an area greater than 96^2 px, AR with a number of detections below 100, AR with a number of detections below 10, and AR with only one detection. This would enable improved distinction between models, as certain datasets may contain a higher proportion of smaller items compared to others. Calculations for precision and recall can be performed in this scenario. The AP and AR curves can be obtained by performing several computations and trials for each class. The AP value corresponds to the area under the curve. The mean average precision (mAP) for object detection is computed by taking the average of the average precision (AP) values derived for each individual class, as demonstrated in the formula below:

$$mAP = \frac{1}{|Q_r|} \sum_{q \in Q_R} AP(q), \quad (13)$$

where Q is the number of queries.

Computer Configuration

Collaboratory, often known as Colab, is an artificial intelligence platform that operates within a web browser. It enables users to create and run Python code notebooks. It will allow us to execute our code on a GPU without any cost.

Statistical Analysis

The results of isolation were repeated three times, results are mean ± standard deviation. The statistical analysis was done by SPSS 25.

RESULTS

Isolation of Fungal Strains

In this study, the five fungal species *Aspergillus terreus, Aspergillus fumigatus, Aspergillus flavus, Aspergillus welwitschiae,* and *Aspergillus austwickii* were isolated and purified as shown in Figure 3. The identification of the isolates was further confirmed using nuclear ribosomal DNA internal transcribed spacer (ITS) for sequencing the PCR products. The obtained nucleotide sequence was deposited at the NCBI GenBank, and a strain identifier was given to each isolate. Thus, they were identified as *Aspergillus terreus*, *Aspergillus fumigatus*, *Aspergillus flavus*, *Aspergillus welwitschiae*, and *Aspergillus austwickii* with accession numbers OQ553958.1, OQ798895.1, OQ798898.1, OQ798899.1, and OQ798926.1, respectively. The dendrogram was established (Figure 13) to show sequence alignments with available sequences from the NCBI data bank.

Aspergillus flavus **GenBank: OQ553958.1** *Aspergillus flavus* isolate AS1 internal transcribed spacer 1, partial sequence; 5.8S ribosomal RNA gene, complete sequence; and internal transcribed spacer 2, partial sequence.

Aspergillus austwickii **GenBank: OQ798895.1** *Aspergillus austwickii* isolate AS2 internal transcribed spacer 1, partial sequence; 5.8S ribosomal RNA gene, complete sequence; and internal transcribed spacer 2, partial sequence.

Aspergillus fumigatus **GenBank: OQ798898.1** *Aspergillus fumigatus* isolates AS3 internal transcribed spacer 1, partial sequence; 5.8S ribosomal RNA gene, complete sequence; and internal transcribed spacer 2, partial sequence.

Aspergillus terreus **GenBank: OQ798899.1** *Aspergillus terreus* isolate AS4 internal transcribed spacer 1, partial sequence; 5.8S ribosomal RNA gene, complete sequence; and internal transcribed spacer 2, partial sequence

Aspergillus welwitschiae **GenBank: OQ798926.1** *Aspergillus welwitschiae* isolate AS5 internal transcribed spacer 1, partial sequence; 5.8S ribosomal RNA gene, complete sequence; and internal transcribed spacer 2, partial sequence

Model Training

Figure 4 and Figure 5 show the mAP@0.5-0.95 and mAP@0.5, respectively. Figure 6 shows the loss, after 10 epochs, the average loss dropped below 2.0, and

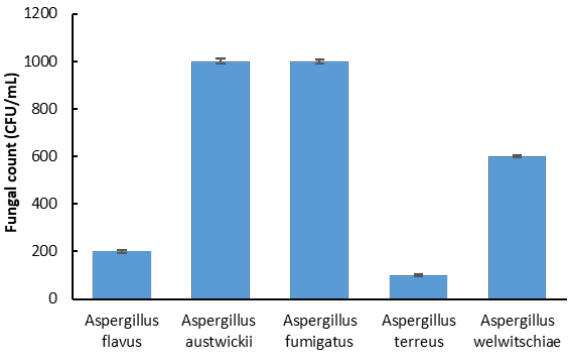

Figure 3. Fungi count (CFU/mL) isolated from soil.

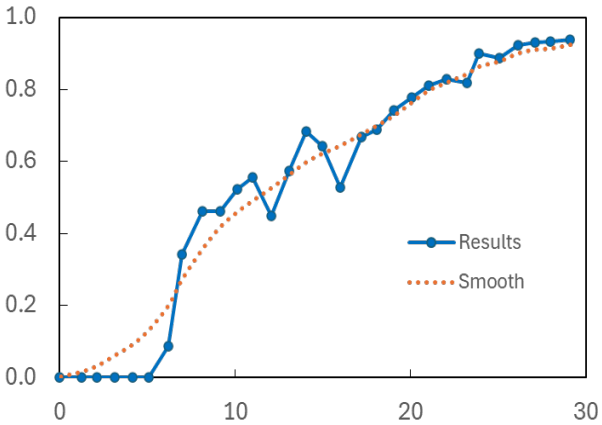

Figure 4. mAP50-95 for the model with batches

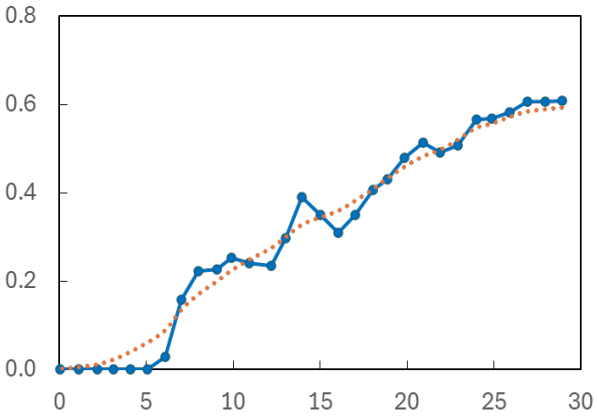

Figure 5. mAP50 for the model with batches.

mAP@0.5-0.95 and mAP@0.5 stabilized quickly, eventually reaching almost 0.6 and 0.9, respectively.

Predictions

The predictions measures illustrated through (Figure 7 - Figure 12) demonstrate the accuracy of our Faster R-CNN model in handling various levels of crowd, backdrops, combinations, and multiple types, as depicted in (Figure 14, Figure 15, and Figure 16). Nevertheless, it has difficulties in accurately identifying *Aspergillus flavus* when there are numerous predictions in an image or when they are positioned as depicted in Figure 14. The predictions made by YOLOv8 regarding all varieties of fungi, even the different types, were incredibly accurate.

DISCUSSION

The identification of unknown *Aspergillus* clinical isolates to the species level is crucial, as different species exhibit varying susceptibilities to numerous antifungal agents(Yang et al., 2024). One of the oldest and most widely used methods in the identification of various *Aspergillus* species is based on their morphological characteristics, such as the color of their colonies and the appearance of their reverse side (Ouf et al., 2019). The morphological characteristics of certain *Aspergillus* species are similar, which makes it challenging to differentiate between them (Ali et al., 2015). Additionally, it is a time-consuming procedure that may not be entirely accurate (Suleiman, 2023). The process of genomes sequencing would be time intensive while also expensive (Rezapour et al., 2023). This work involved the training and testing of a model specifically designed for the identification of *Aspergillus*. Their performances were evaluated by recognizing 5 distinct kinds of *Aspergillus*, some of which exhibit close resemblances in terms of forms and colors against diverse backdrops in several photographs. Small object detection has consistently been a focal point of research in the field of object detection.

The fungal detection using macroscopic detection in the past was difficult since it looks similar even if it belongs to different *Aspergillus* fungi species, we genetically identified the fungal DNA results, and the results were submitted to GenBank. This study employed object detection models to precisely recognize and locate *Aspergillus*. The training stage of YOLOv8 included mosaic data augmentation, which combined four photos into a single image. Utilizing mosaic data augmentation has demonstrated its efficacy in enhancing the recognition of different species of *Aspergillus* in our dataset, as well as detecting closely *Aspergillus* resembling forms with similar coloration. Deep learning was used in several research projects to identify and detect fungi. Recent works have used deep learning approaches to detect illness and classify and observe several *Aspergillus* species. The diagnosis of invasive aspergillosis infection is complex and necessitates a practical, effective, and economical approach.

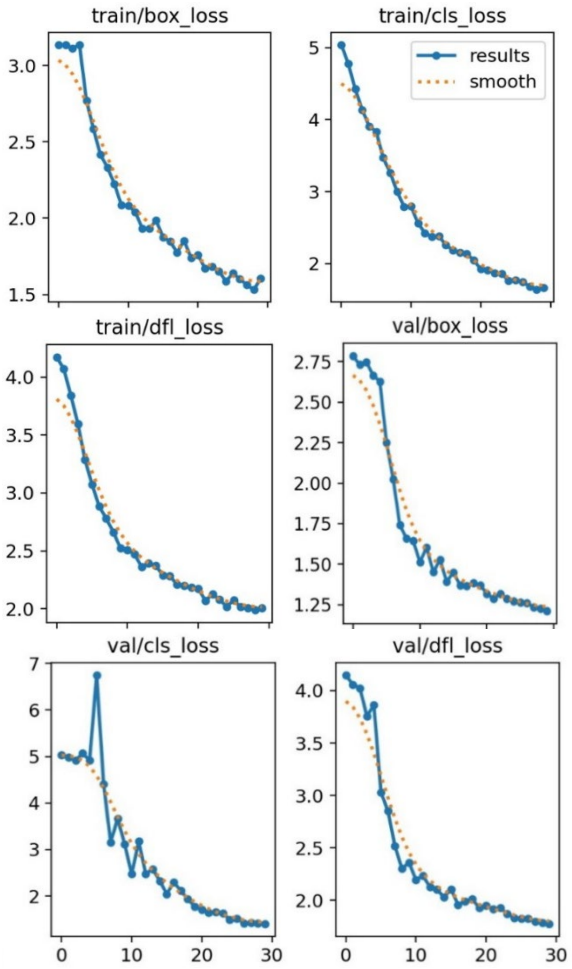

Figure 6. Loss functions for the YOLOv8 model.

The study explores the capacity of infrared spectroscopy, in conjunction with machine learning, to meet this therapeutic requirement. Two sets of infrared spectrum data were utilized in this study. The first set consisted of nine plasma samples spiked with *Aspergillus* and seven *Aspergillus*-free plasma samples. The second set was constructed by oversampling these sixteen samples, resulting in 200 spectral data points. Two models were trained using Partial Least Squares-Discriminant Analysis (PLS-DA). In addition, two other models were trained using the same data. However, prior to performing PLS-DA, autoscaling was performed. Forty-five fictitious samples that mimicked the complex samples of patients at risk of invasive aspergillosis were used to evaluate these models. These samples included the presence of medications (9 tested) and other common infections (5 tested) as potential confounders. The accuracy of the simple model's predictions is 84.4%, but it may be increased to 93.3% by applying autoscaling and oversampling.

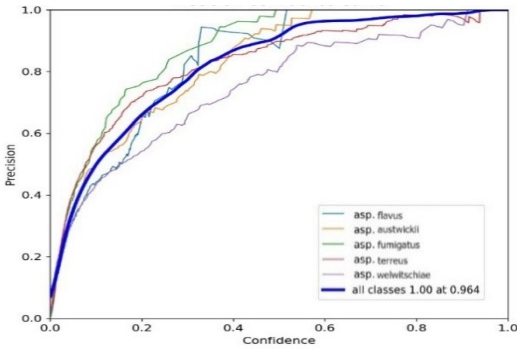

Figure 7. Precision-confidence curve.

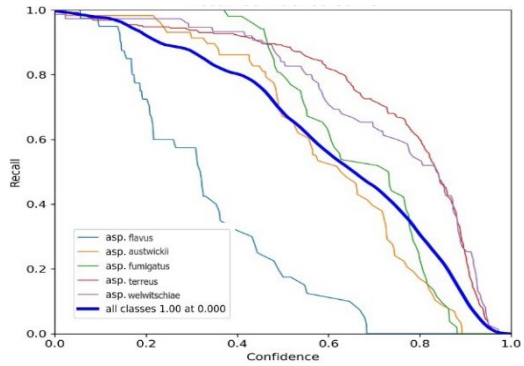

Figure 8. Recall-confidence curve.

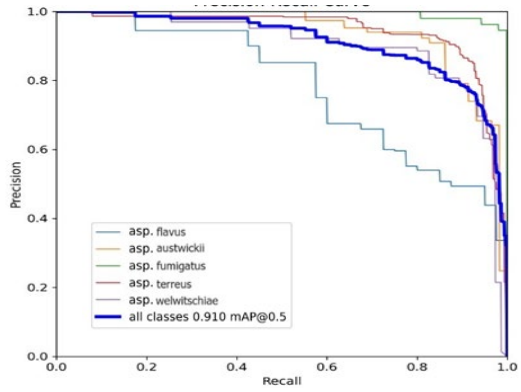

Figure 9. Precision-recall curve.

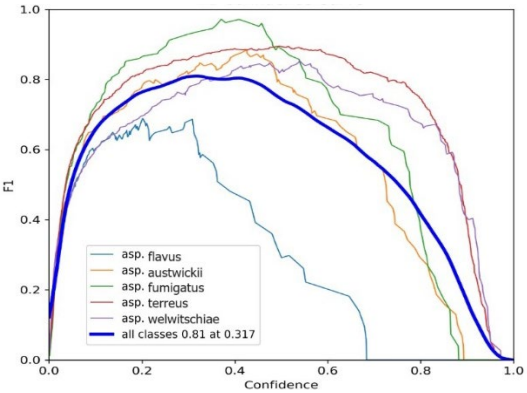

Figure 10. F1-confidence curve.

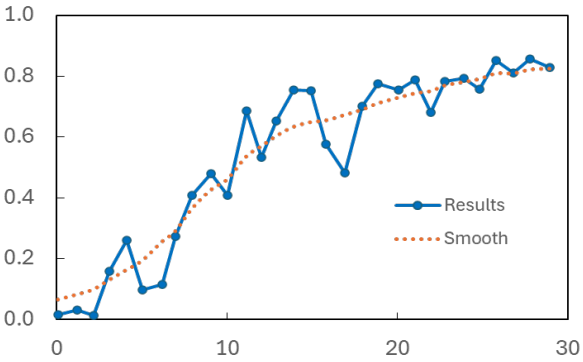

Figure 11. Recall(B).

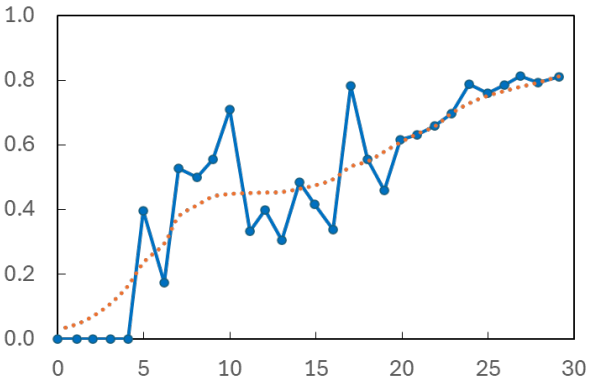

Figure 12. Precision(B).

The study's findings indicate that *Aspergillus* species can be identified in blood plasma by infrared spectroscopy, even, when possible, confounders frequently seen in the blood of patients at risk of invasive aspergillosis are present (Elkadi et al., 2021).

This study describes a method for classifying *Aspergillus* fungus species under the microscope. The authors of a different research paper explained how to identify fungi from macroscopic photos (Campbell and Johnson, 2013). On the other hand, certain *Aspergillus* fungi appear identical in macroscopic pictures despite belonging to different species. This paper describes a procedure for the microscopic identification and categorization of a species of *Aspergillus* fungal species belonging to the 9 types (Khalil et al., 2016). Four thousand five hundred forty-five microscopic photos are used to train and evaluate a machine learning model. In training, the CNN model v1 had an accuracy of 87.50%, and in validation, it had an accuracy of 95.65%. To enhance training performance, the model is recalculated. The CNN model v1.1 dropped the dropout rate from 0.5 to 0.2 and substituted SoftMax activation for sigmoid activation. 94.20% accuracy in training and 94.31% accuracy in validation were attained by the recalibrated model (Billones et al., 2020).

Since *Aspergillus* species are widely dispersed in nature and some can cause invasive aspergillosis (IA) infections in immunocompromised individuals as well as contamination in agricultural products, automated and economical methods are required for the most labor-intensive and operator-dependent processes, such as microscopic observation and molecular detection of *Aspergillus* species. To tackle this difficulty, the capacity to categorize different *Aspergillus* species was investigated using a deep convolutional neural network (CNN). A 35× objective was used to scan colonies on plates using a dissecting microscopy (DM)/stereomicroscopy platform, producing pictures with enough resolution for categorization. The typical representative shape of conidiophores or colonies of each strain was captured in 17,142 picture crops that were created as training and test datasets using 8,995 original colony photographs from seven *Aspergillus* species grown in enrichment media. Positively, the training picture collection showed that the Xception model had a 99.8% classification accuracy.

On the test picture set, our CNN model's classification accuracy after training was 99.7%. This classification system was also employed to identify and validate a fresh collection of raw photos of these strains, demonstrating a detection accuracy of 98.2% based on the Xception performance during training and testing. As a result, our research presented a fresh idea for an affordable, artificial intelligence-based approach to *Aspergillus* organism detection that may help increase public awareness of the fungus kingdom (Ma et al., 2021).

This study uses transfer learning with convolutional neural networks (CNNs) to handle the problem of reliably recognizing filamentous fungi in the medical laboratory. The analysis classifies fungal taxa and identifies *Aspergillus* species using microscopic pictures from touch-tape slides stained with lactophenol cotton blue, the most widely used technique in clinical settings. Four thousand one hundred eight photos with typical microscopic morphology for each genus were included in the training and test datasets, and to improve classification accuracy, a soft attention mechanism was included. Thus, the study's total classification accuracy was 94.9% for four commonly seen genera and 84.5% for species of *Aspergillus*. One of its unique aspects is that medical technicians were involved in developing a model that easily fits into regular processes.

Figure 13: Phylogenetic trees describing sequence alignment with available sequences from the NCBI data bank of a) Phylogenetic tree of Aspergillus flavus, b) Phylogenetic tree of Aspergillus austwickii. C) phylogenetic tree of Aspergillus fumigatus, d) Phylogenetic tree of Aspergillus terreus and e) Phylogenetic tree of Aspergillus welwitschiae.

Furthermore, the study emphasizes how precise and effective filamentous fungal diagnosis may be achieved by combining cutting-edge technology with established medical laboratory procedures (Huang et al., 2023).

One of the well-known saprophytic fungi that can survive in a variety of conditions is *Aspergillus*. Although some can be useful in the food sector, others can infect humans and animals, usually targeting individuals with weakened immune systems. To maintain treatment continuity with more precise analysis, *Aspergillus* identification is crucial. *Aspergillus* can only be identified by its characteristics; now, two approaches are employed to examine these characteristics: microscopic and macroscopic analyses.

Before delivering the final outcomes, a few verifications must be made by skilled microscopists. Consequently, an automation-based identification is suggested to avoid misidentification. This study compares and tests various supervised classifiers to see how well they can identify 162 distinct *Aspergillus* pictures. Principal component analysis (PCA) was used to extract the features, and several classifiers were used, including Improved Fuzzy-Based k Nearest Centroid Neighbor (IFkNCN), Sparse Representation Classifier (SRC), Support Vector Machine (SVM), and Kernal Sparse Representation Classifier (KSRC).

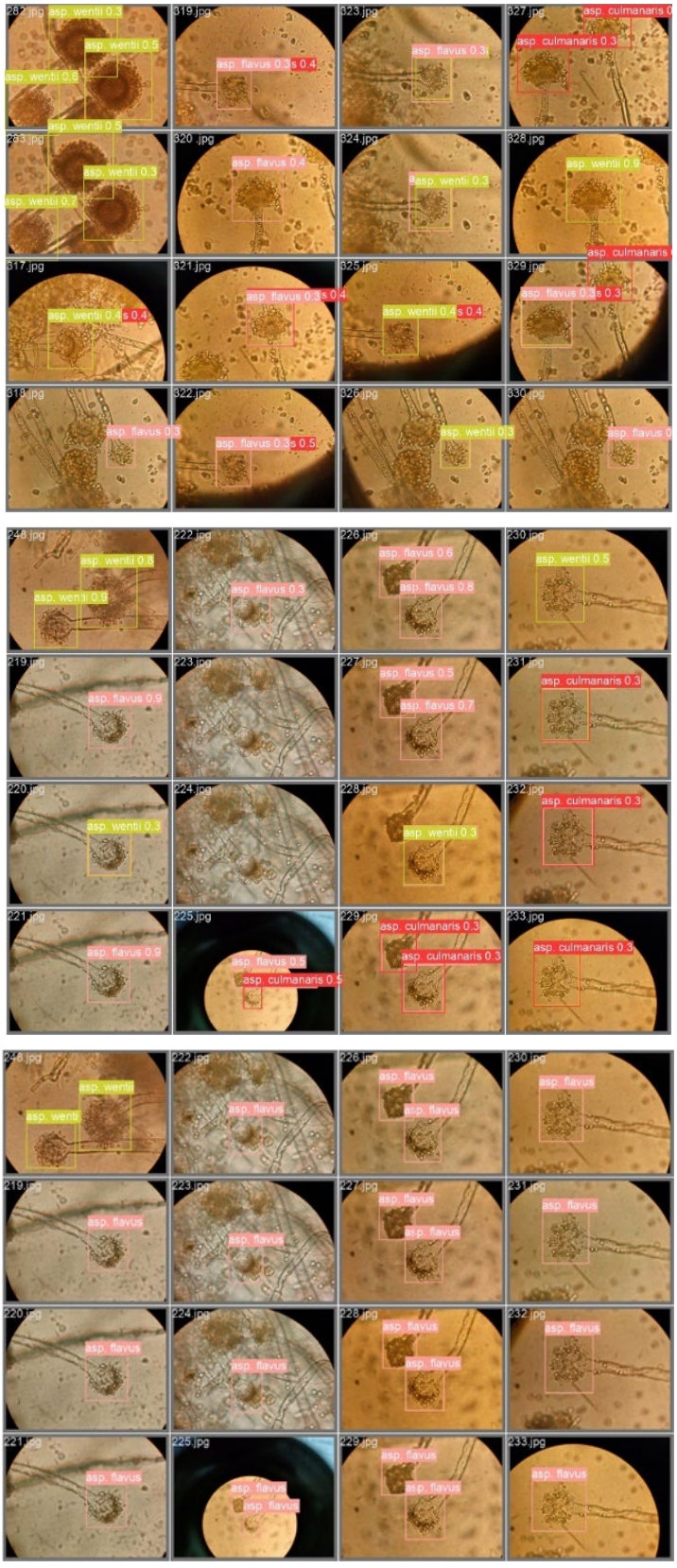

Figure 14. YOLOv8 predictions with *Aspergillus flavus*.

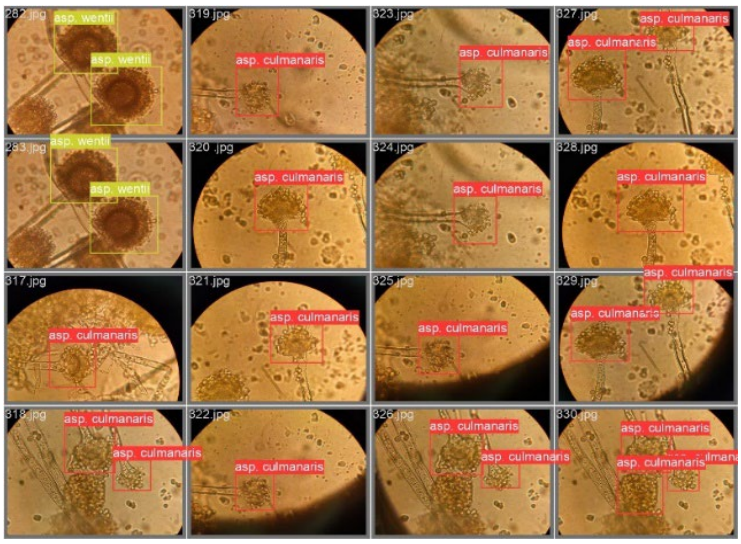

Figure 15. YOLOv8 predictions with *Aspergillus austwickii*.

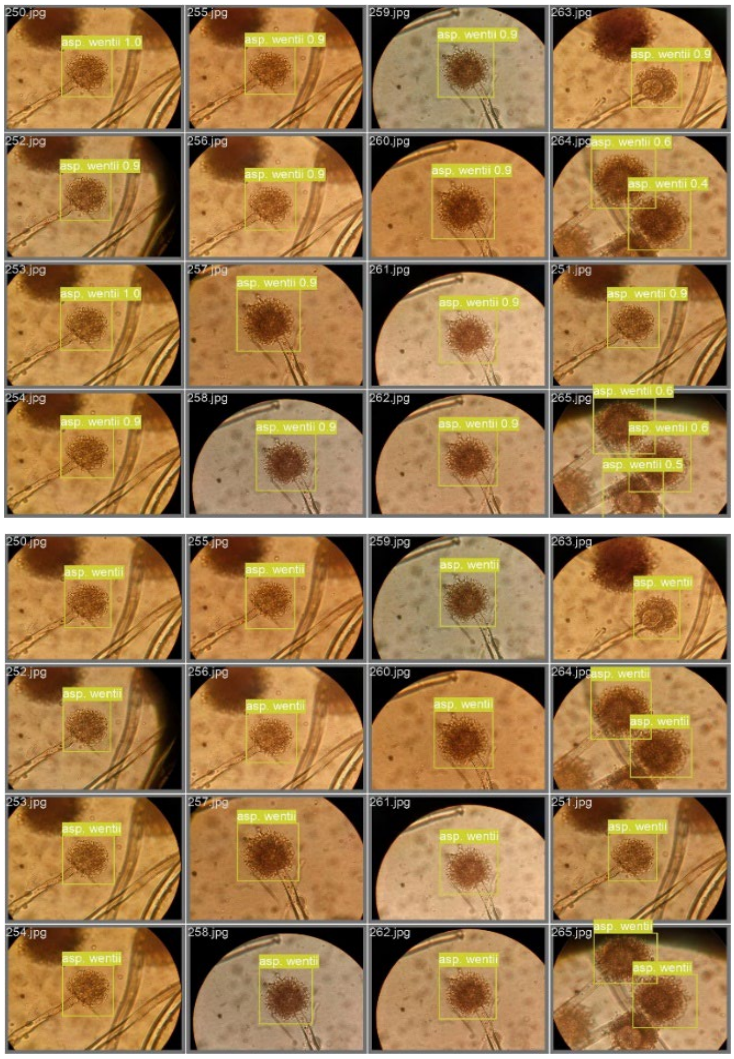

Figure 16: YOLOv8 predictions with Aspergillus welwitschiae.

Aspergillus flavus achieved 80% accuracy across all classifiers based on its accuracy (Radzuan et al., 2022).

CONCLUSION

The *Aspergillus* dataset was gathered for this study, and a deep learning model was created using transfer learning techniques. The YOLOv8 model achieves satisfactory accuracy and runtime performance while requiring a lower computational load. The approach can be utilized for the detection of *Aspergillus* in diverse intricate contexts, encompassing different sizes and multiangle settings. The YOLOv8 model, with an error rate of less than 2% and a running time of less than 2 seconds, is a highly effective technique for detecting *Aspergillus*. Subsequent efforts will improve the construction of more extensive datasets and the evaluation methods to enhance the model's optimization and enhance the accuracy and efficiency of detection. Furthermore, the existing research can be expanded to encompass the identification of different types of *Aspergilli*, the real-time detection and quantification of *Aspergillus*, and the automation of various microbiology detection procedures.

ACKNOWLEDGEMENTS

The authors are grateful to Eng. Noran S. Ouf for providing the idea and the method used in this manuscript. She has been a source of inspiration through her own research.

REFERENCES

Ali, M.I.A.; Ouf, S.A.; Khalil, N.M.; Abd El-Ghany, M.N. Biosynthesis of laccase by *Aspergillus flavus* NG85 Isolated from Saint Catherine protectorate. *Egyptian Journal of Botany* 2015, *55*, 127–147.

Al-Ameri, H. A. (2024). Molecular Identification of *Aspergillus* spp. isolated from different vegetables in markets of Dohuk city/Iraq. *Journal of Applied and Natural Science*, *16*(2), 722–729. https://doi.org/10.31018/jans.v16i2.5449

Asnicar, F., Thomas, A. M., Passerini, A., Waldron, L., & Segata, N. (2024). Machine learning for microbiologists. *Nature Reviews Microbiology*, *22*(4), 191–205. https://doi.org/10.1038/s41579-023-00984-1

Balajee, S. A., Houbraken, J., Verweij, P. E., Hong, S. B., Yaghuchi, T., Varga, J., & Samson, R. A. (2007). *Aspergillus* species identification in the clinical setting. *Studies in Mycology*, *59*, 39–46. https://doi.org/10.3114/sim.2007.59.05

Billones, R. K. C., Calilung, E. J., Dadios, E. P., & Santiago, N. (2020, December 3). *Aspergillus* Species Fungi Identification Using Microscopic Scale Images. *2020 IEEE 12th International Conference on Humanoid, Nanotechnology, Information Technology, Communication and Control, Environment, and Management, HNICEM 2020*. https://doi.org/10.1109/HNICEM51456.2020.9400039

Bochkovskiy, A., Wang, C. Y., & Liao, H. Y. M. (2020). Yolov4: Optimal speed and accuracy of object detection. arXiv preprint arXiv:2004.10934.

Camargo, A., & Smith, J. S. (2009). Image pattern classification for the identification of diseases causing agents in plants. *Computers and Electronics in Agriculture*, *66*(2), 121–125. https://doi.org/10.1016/j.compag.2009.01.003

Campbell, C. K., & Johnson, E. M. (2013). Identification of pathogenic fungi. John Wiley & Sons.

Diba, K., Kordbacheh, P., Mirhendi, S. H., Rezaie, S., & Mahmoudi, M. (2007a). Identification of *Aspergillus* species using morphological characteristics. *Pakistan Journal of Medical Sciences*, *23*(6), 867–872. https://doi.org/10.1007/s12043-002-0227-9

Diba, K., Kordbacheh, P., Mirhendi, S. H., Rezaie, S., & Mahmoudi, M. (2007b). Identification of *Aspergillus* species using morphological characteristics. *Pakistan Journal of Medical Sciences*, *23*(6), 867–872. https://doi.org/10.1007/s12043-002-0227-9

Dobiáš, R., Stevens, D. A., & Havlíček, V. (2023). Current and Future Pathways in *Aspergillus* Diagnosis. *Antibiotics*, *12*(2), 385. https://doi.org/10.3390/antibiotics12020385

Elkadi, O. A., Hassan, R., Elanany, M., Byrne, H. J., & Ramadan, M. A. (2021). Identification of *Aspergillus* species in human blood plasma by infrared spectroscopy and machine learning. *Spectrochimica Acta - Part A: Molecular and Biomolecular Spectroscopy*, *248*. https://doi.org/10.1016/j.saa.2020.119259

Gilman, J. (1957). A manual of soil fungi. *Soil Science*, *84*, 1–183.

Guzella, T. S., & Caminhas, W. M. (2009). A review of machine learning approaches spam filtering. *Expert Systems with Applications*, *36*(7), 10206–10222. https://doi.org/10.1016/J.ESWA.2009.02.037

Huang, H., Xu, H., Wang, X., & Silamu, W. (2015). Maximum F1-score discriminative training criterion for automatic mispronunciation detection. *IEEE/ACM Transactions on Audio Speech and Language Processing*, *23*(4), 787–797. https://doi.org/10.1109/TASLP.2015.2409733

Huang, T.-S., Wang, K., Ye, X.-Y., Chen, C.-S., & Chang, F.-C. (2023). Attention-Guided Transfer Learning for Identification of Filamentous Fungi Encountered in the Clinical Laboratory. *Microbiology Spectrum*, *11*(3). https://doi.org/10.1128/spectrum.04611-22

Johnson, L. F. and C. E. A. and B. J. H. and F. H. A. (1960). *Methods for studying soil microflora-plant disease relationships.* 178.

Khalil NK, Ali MI, Ouf SA, Abd El-Ghany MN (2016) Characterization of Aspergillus flavus NG 85 laccase and its dye decolorization efficiency. Research Journal of Pharmaceutical, Biological and Chemical Sciences 7(4): 829–817.

Khalil, N. M., Abd El-Ghany, M. N., & Rodríguez-Couto, S. (2019). Antifungal and anti-mycotoxin efficacy of

biogenic silver nanoparticles produced by Fusarium chlamydosporum and Penicillium chrysogenum at non-cytotoxic doses. *Chemosphere*, *218*, 477–486. https://doi.org/10.1016/j.chemosphere.2018.11.129

Ma, H., Yang, J., Chen, X., Jiang, X., Su, Y., Qiao, S., & Zhong, G. (2021). Deep convolutional neural network: a novel approach for the detection of *Aspergillus* fungi via stereomicroscopy. *Journal of Microbiology*, *59*(6), 563–572. https://doi.org/10.1007/s12275-021-1013-z

MacLeod, N. (2017). On the use of machine learning methods in morphometric analysis. *Proceedings of the Fourth International Symposium on Biological Shape Analysis*, 134–171. https://doi.org/10.1142/9789813225701

McClenny, N. (2005). Laboratory detection and identification of *Aspergillus* species by microscopic observation and culture: the traditional approach. *Medical Mycology*, *43*(sup1), 125–128. https://doi.org/10.1080/13693780500052222

Moubasher, A. H. (1993). Soil Fungi in Qatar and Other Arab Countries. *The Centre of Scientific and Applied Research University of Qater*.

Oliveira, M., & Azevedo, L. (2022). Molecular Markers: An Overview of Data Published for Fungi over the Last Ten Years. *Journal of Fungi*, *8*(8), 803. https://doi.org/10.3390/jof8080803

Ouf, Noran, S. (2023). Leguminous seeds detection based on convolutional neural networks: Comparison of Faster R-CNN and YOLOv4 on a small custom dataset. Artificial Intelligence in Agriculture, 8: 30-45.

Ouf SA, El-Yasergy KF, Mohammed HA, Abd El-Ghany MN (2019) Efficacy of ozonized water for fungal decontamination of fresh fruit pieces decorating dessert cakes. Egypt J Bot 59(3):845–855

Perrone, G., Susca, A., Cozzi, G., Ehrlich, K., Varga, J., Frisvad, J. C., Meijer, M., Noonim, P., & Mahakarnchanakul, W. (2007). Biodiversity of *Aspergillus* species in some important agricultural products. *Studies in Mycology*, *59*, 53–66. https://doi.org/10.3114/sim.2007.59.07

Qi, G., Hao, L., Gan, Y., Xin, T., Lou, Q., Xu, W., & Song, J. (2024). Identification of closely related species in *Aspergillus* through Analysis of Whole-Genome. *Frontiers in Microbiology*, *15*, 1323572. https://doi.org/10.3389/fmicb.2024.1323572

Qiu, Z., Chen, J., Zhao, Y., Zhu, S., He, Y., & Zhang, C. (2018). Variety Identification of Single Rice Seed Using Hyperspectral Imaging Combined with Convolutional Neural Network. *Applied Sciences*, *8*(2), 212. https://doi.org/10.3390/app8020212

Radzuan, N. R. R. binti M., Jaafar, H. B., & Nasir, A. S. B. A. (2022). An Identification of *Aspergillus* Species: A Comparison on Supervised Classification Methods. *Lecture Notes in Electrical Engineering*, *770*, 965–977. https://doi.org/10.1007/978-981-16-2406-3_71

Rakiya, A., Kellu, H. A., Oyekemi, A. O., & Benisheikh, A. A. G. (2024). Isolation and Morphological Identification of *Aspergillus* Species from Some Cultivated Soils in Maiduguri, Nigeria. https://doi.org/10.3923/rjm.2024.1.8

Raper, K. (1965). The Genus *Aspergillus*. *The Williams and Wilkins Co*.

Rezapour, A., Souresrafil, A., Barzegar, M., Sheikhy-Chaman, M., & Tatarpour, P. (2023). Economic evaluation of next-generation sequencing techniques in diagnosis of genetic disorders: A systematic review. *Clinical Genetics*, *103*(5), 513–528. https://doi.org/10.1111/cge.14313

Suleiman, W. B. (2023). A multi-aspect analysis of two analogous *Aspergillus* spp. belonging to section Flavi: *Aspergillus* flavus and *Aspergillus* oryzae. *BMC Microbiology*, *23*(1), 71. https://doi.org/10.1186/s12866-023-02813-0

Watanabe, T. (2002). Pictorial atlas of soil and seed fungi: morphologies of cultured fungi and key to species. *CRC Press*.

WU, W., YANG, T. le, LI, R., CHEN, C., LIU, T., ZHOU, K., SUN, C. ming, LI, C. yan, ZHU, X. kai, & GUO, W. shan. (2020). Detection and enumeration of wheat grains based on a deep learning method under various scenarios and scales. *Journal of Integrative Agriculture*, *19*(8), 1998–2008. https://doi.org/10.1016/S2095-3119(19)62803-0

Yang, Z., Qiao, Y., Strøbech, E., Morth, J. P., Walther, G., Jørgensen, T. S., Lum, K. Y., Peschel, G., Rosenbaum, M. A., Previtali, V., Clausen, M. H., Lukassen, M. V., Gotfredsen, C. H., Kurzai, O., Weber, T., & Ding, L. (2024). Alligamycin A, an antifungal β-lactone spiroketal macrolide from Streptomyces iranensis. *Nature Communications*, *15*(1), 9259. https://doi.org/10.1038/s41467-024-53695-3.